Chemical Engineering Journal 397 (2020) 125501

Contents lists available at ScienceDirect

Chemical Engineering Journal

journal homepage: www.elsevier.com/locate/cej

Acceleration of peroxymonosulfate decomposition by a magnetic MoS_2/$CuFe_2O_4$ heterogeneous catalyst for rapid degradation of fluoxetine

Rui Bai[a,b], Weifu Yan[a], Yong Xiao[a,*], Siqi Wang[c], Xiaochun Tian[a], Junpeng Li[a,b], Xiaofeng Xiao[a,b], Xiaoquan Lu[c,d], Feng Zhao[a,*]

[a] CAS Key Laboratory of Urban Pollutant Conversion, Institute of Urban Environment, Chinese Academy of Sciences, Xiamen 361021, China
[b] University of Chinese Academy of Sciences, Beijing 100049, China
[c] Key Laboratory of Bioelectrochemistry & Environmental Analysis of Gansu Province, College of Chemistry & Chemical Engineering, Northwest Normal University, Lanzhou, 730070, China
[d] Tianjin University, Tianjin 300072, China

HIGHLIGHTS

- $CuFe_2O_4$ was uniformly doped onto MoS_2 to activate peroxymonosulfate.
- Hydroxyl radicals and sulfate radicals were the major reactive oxygen species.
- Efficient degradation was ascribed to the rapid decomposition of peroxymonosulfate.
- Nine intermediates involving hydroxylation and open-chain or -ring were detected.

ARTICLE INFO

Keywords:
Molybdenum disulfide
Copper ferrite
Peroxymonosulfate
Fluoxetine
Electron transfer

ABSTRACT

By modifying copper ferrite on the surface of molybdenum disulfide (MoS_2/$CuFe_2O_4$), an excellent catalyst that can be used for interaction with peroxymonosulfate was successfully synthesized. Owing to the large number of active sites (unsaturated sulfur) on the surface of the composite material, the electron transfer and decomposition rate of the oxidant in the reaction system were significantly enhanced. The removal ability was the strongest when the molar ratio of MoS_2/$CuFe_2O_4$ was 1.5. The removal efficiency of fluoxetine reached 97.7% within 20 min, which was higher than those obtained by pure MoS_2 (38.6%) and $CuFe_2O_4$ (22.1%). The free radical test and electron paramagnetic resonance analysis indicated that sulfate radicals and hydroxyl radicals were the dominant reactive oxygen species in the reaction system. In addition, in situ Raman spectroscopy revealed that peroxymonosulfate was rapidly decomposed in the composite material system. Meanwhile, the degradation products of fluoxetine were explored by high-performance liquid chromatography-tandem mass spectrometry, and a transformation pathway based on nine intermediates was proposed, mainly involving the breaking of the carbon-oxygen bond around oxygen atom, hydroxylation, and ring-opening reactions of fluoxetine and its intermediates.

1. Introduction

Pollution of freshwater systems worldwide by thousands of industrial and natural compounds has become a major environmental problem [1]. Pharmaceuticals and personal care products, as some of the most concerning emerging pollutants, have been widely detected in natural water in recent years [2]. Fluoxetine, which is a typical, widely used antidepressant, has long-term effects of biological accumulation and toxicity to aquatic life even at low concentrations in the environment [3]. However, traditional sewage treatment processes can no longer handle the increasing impact of refractory pollutants because of their complex structures and high stability [1,4]. Therefore, it is necessary to explore new water treatment technologies to address such contaminants.

Advanced oxidation processes are widely used to remove organic pollutants owing to their strong ability to decompose pollutants by

* Corresponding authors.
E-mail addresses: yxiao@iue.ac.cn (Y. Xiao), fzhao@iue.ac.cn (F. Zhao).

https://doi.org/10.1016/j.cej.2020.125501
Received 15 February 2020; Received in revised form 8 May 2020; Accepted 14 May 2020
Available online 15 May 2020
1385-8947/

generating free radicals [5]. Compared with the traditional Fenton reaction, sulfate radical ($SO_4^{\cdot -}$)-based advanced oxidation processes can generate more active radicals ($SO_4^{\cdot -}$ with 2.5–3.1 V/NHE vs. $^{\cdot}OH$ with 2.5V/NHE) [6,7]. Another advantage is that it can adapt to a wider pH range compared with the strict acidic conditions required for the Fenton reaction. A series of methods, including UV [8], thermal [9], ultrasound [10], and transition metals [11–13], have been used to activate peroxymonosulfate to generate active O species. However, some drawbacks can be observed in the UV, thermal, and ultrasound methods, such as high cost and relatively complex operation. In recent decades, considerable development has been achieved regarding transition metal-based materials. Among the various transition metal oxides, copper ferrite ($CuFe_2O_4$), as a typical material of spinel ferrite, has attracted great interest in the activation process of heterogeneous peroxymonosulfate owing to its high stability and environmental friendliness as well as its reactive activity [14]. In addition, $CuFe_2O_4$ can be separated from water by a magnet. Thus, the integration of $CuFe_2O_4$ with peroxymonosulfate has considerable potential for oxidation and removal of organic contaminants. However, developing methods for enhancing the utilization rate of peroxymonosulfate and for avoiding material aggregation and further obtaining a higher activation efficiency are two major issues that need to be addressed in this advanced oxidation process.

Molybdenum disulfide (MoS_2) is widely used in field photocatalysis and electrocatalysis because of its abundant active sites and high electron mobility [15]. Recently, Xing et al. [16,17] introduced Mo-based catalysts into the Fenton system and clarified that MoS_2 not only plays an important role in repairing the activity of catalysts, but also accelerates the decomposition of oxidants. In addition, Sheng et al. [18] added MoS_2 to the conventional Fe(II)/peroxymonosulfate system and found that the boost in catalytic performance and the Fe(III) formed after the reaction could be quickly reduced to Fe(II) by MoS_2, which further improved the utilization rate of oxidants. Meanwhile, the presence of unsaturated S enables MoS_2 to have reduction properties and can transfer electrons to peroxymonosulfate molecule. However, MoS_2 also has some disadvantages that limit its practical application, such as a short charge transfer and poor conductivity [19,20]. However, what the role of molybdenum disulfide that is clear only in Fe(II)/H_2O_2 and Fe(II)/peroxymonosulfate systems Therefore, to overcome the various defects of $CuFe_2O_4$ and MoS_2, we compounded $CuFe_2O_4$ and MoS_2 expecting that the decomposition rate of peroxymonosulfate and the electron transfer capacity between the metal elements near the S vacancies and peroxymonosulfate would be greatly improved from the following considerations. On one hand, the aggregation of magnetic $CuFe_2O_4$ would be alleviated, which would ensure its good dispersion on the surface of MoS_2. On the other hand, the composite material would still maintain a favorable magnetic quality, which plays a significant role in its recovery and reuse.

In the present study, we synthesized $MoS_2/CuFe_2O_4$ using a two-step reaction method and activated peroxymonosulfate with the generation of free radicals for the first time. Fluoxetine was chosen as the target contaminant to estimate the catalytic ability of the $MoS_2/CuFe_2O_4$/peroxymonosulfate system [21]. The effects of various parameters, including the catalyst dosage, peroxymonosulfate concentration, ratio of $MoS_2/CuFe_2O_4$, and presence of inorganic ions (nitrate (NO_3^-), sulfate (SO_4^{2-}), carbonate (CO_3^{2-}), chloride (Cl^-)) and natural organic matter (humic acid), on the removal of fluoxetine were investigated. In addition, the reaction species were also investigated by quenching experiments and electron paramagnetic resonance analysis. Meanwhile, the decomposition rate of peroxymonosulfate was also detected by in situ Raman spectroscopy. Finally, liquid chromatography-tandem mass spectrometry (LC-MS/MS) was used to determine the degradation intermediates of fluoxetine under the $MoS_2/CuFe_2O_4$/peroxymonosulfate degradation system.

2. Materials and methods

2.1. Chemicals and materials

Fluoxetine hydrochloride was purchased from Aladdin Industrial Corporation (China; purity > 98.5%). Potassium peroxymonosulfate ($2KHSO_5{\cdot}KHSO_4{\cdot}K_2SO_4$) was purchased from Alfa Aesar (Germany; purity > 98.5%). Methanol and acetonitrile (high-performance liquid chromatography (HPLC) grade) were ordered from Merck KGaA (Germany). All the other chemicals (analytical grade) were purchased from Sinopharm Group Co., Ltd. (Shanghai, China).

2.2. Preparation of $MoS_2/CuFe_2O_4$

$CuFe_2O_4$ nanoparticles were prepared according to our previous study [22]. Briefly, $Cu(NO_3)_2{\cdot}3H_2O$ and $Fe(NO_3)_3{\cdot}9H_2O$ were dissolved in ultrapure water and guaranteed the molar ratio of Cu to Fe of 1:2, and a magnetic stirrer was used to stir the solution for 2 h at 60 °C. Equimolar citric acid and metal cations was then added and stirred at 60 °C for 2 h. The homogeneous solution was evaporated at 125 °C for 14 h in an oven to remove water, and then a nitric acid-citric acid composite gel was calcined at 400 °C for 2 h to decompose the citric acid.

$MoS_2/CuFe_2O_4$ nanocomposites was synthesized using a modified two-step hydrothermal method [23]. First, 0.17 mmol of $(NH_4)_6Mo_7O_{24}{\cdot}4H_2O$ and 6.00 mmol of thiourea were dissolved together in 30 mL of distilled water and stirred for 30 min. The mixture was then dispersed by ultrasound after adding a certain amount of as-prepared $CuFe_2O_4$. The obtained solution was subsequently transferred to a 50 mL Teflon-lined stainless-steel autoclave and maintained at 180 °C for 10 h. After the reaction system cooled, the final black products were collected by a magnet, washed three times with distilled water and ethanol, and dried at 60 °C for 24 h under a vacuum. In addition, the marks of MC1, MC1.5, and MC2 indicated that the molar ratio of MoS_2 and $CuFe_2O_4$ were 1:1, 3:2, and 2:1, respectively. We also utilized a similar method to synthesize pure MoS_2.

2.3. Characterization

The X-ray diffraction (XRD) pattern was recorded by an X'pert PRO MPD diffractometer (PANalytical) operating at 40 kV and 40 mA under Cu Kα radiation (λ = 0.15406 nm). Fourier transform infrared (FTIR) spectra were provided by a Thermo Scientific Nicolet spectrophotometer (iS10) with samples embedded in KBr pellets. The morphologies of the samples were determined on a transmission electron microscope (TEM; Tecnai G2 F20). X-ray photoelectron spectroscopy (Kratos Analytical Inc.) with unmonochromatized Al Kα radiation (150 W) as an X-ray source was used to measure the surface chemistry properties, and all the binding energies were calibrated with C1s at 284.8 eV. The charge of as-prepared catalysts was analyzed by zeta potential (Malvern Zeta PALS), the catalysts were dispersed in deionized water and then adjusted the pH (HCl and NaOH) to form solutions at pH values ranging from 3 to 11. Specific surface areas of as-prepared catalysts were measured by N_2 adsorption–desorption experiments at 77 K (Micrometrics Inc., ASAP-2020 M analyzer) using Brunauer-Emmett-Teller (BET) method. The electron paramagnetic resonance spectra of trapped radicals were obtained by a JES FA200 electron paramagnetic resonance (EPR) device, which used 100 mM of 5,5-dimethyl-1-pyrroline N-oxide (DMPO) as a spin-trapping agent to identify the radicals generated from the $MoS_2/CuFe_2O_4$/peroxymonosulfate system. The measurement conditions included a microwave frequency of 9.056 GHz, microwave power of 0.998 mW, and temperature of 25 °C.

2.4. Experimental procedures

To test the catalytic effect of $MoS_2/CuFe_2O_4$ nanocomposites, we chose fluoxetine as a model pollutant. All the experiments were conducted in 150 mL glass beakers containing 80 mL of 20 mg/L fluoxetine and certain quantities of catalyst with continuous stirring with a mechanical mixer at 300 rpm. The reaction was subsequently initiated by adding various amounts of peroxymonosulfate. At each interval, 0.75 mL samples were extracted and immediately quenched by 0.75 mL of methanol, and then the mixture was centrifuged for 10 min at 10 000 rpm to remove the catalyst before the test. Before the reaction, 1 mol/L methanol and *tert*-butanol were added to the system to conduct the free radicals quenching experiment. In addition, various concentrations of NO_3^-, SO_4^{2-}, CO_3^{2-}, Cl^-, and humic acid were added to the system to test their effects on the degradation system. The total organic carbon of the sample was determined by a Shimadzu TOC-VWP analyzer. The concentration of leached ions after reaction was detected by inductively coupled plasma optical emission spectrometer (PerkinElmer Optima 7000DV)

2.5. Analysis method

An HPLC system (L-2000, Hitachi, Japan) equipped with a UV detector and Agilent column (Zorbax Eclipse Plus C18; 4.6 × 250.0 mm; 5 μm) was used to measure the concentration of fluoxetine. The mobile phases consisted of 10 mmol/L of potassium dihydrogen phosphate (phase A, pH adjusted to 3 by phosphoric acid) and acetonitrile (phase B) (55/45; v/v). In addition, the wavelength of detection was 227 nm and the temperature of the column was set at 25 °C. The degradation byproducts of fluoxetine were measured by an ultra-HPLC system (Ultimate 3000) with MS (Thermo Scientific Q Exactive). A C18 column (2.1 × 50.0 mm; 1.8 μm; Agilent ZORBAX Eclipse XDB) was used for separation, and the detection wavelength was set from 210 nm to 254 nm. In addition, the mass spectra were obtained in positive electrospray (ESI +) and negative electrospray (ESI-) mode with *m/z* ranging from 50 to 750.

3. Results and discussion

3.1. Characterization of catalysts

XRD patterns of prepared $MoS_2/CuFe_2O_4$ nanocomposites are shown in Fig. 1a. The main peaks at 2θ at 14.46°, 29.12°, 32.96°, 38.15°, 47.90°, 51.85°, and 58.15° corresponded to the (0 0 3), (0 0 6), (1 0 1), (1 0 4), (1 0 7), (0 1 8), and (1 1 0) planes of MoS_2, respectively, which matched well with PDF no. 089-3040. Meanwhile, the peaks at 18.33°, 30.17°, 35.54°, 43.43°, 47.30°, and 62.74° could be assigned to (1 1 1), (2 2 0), (3 1 1), (4 0 0), (3 3 1), and (4 4 0) of $CuFe_2O_4$ indexed to PDF no. 077-0010. The XRD patterns indicated that $CuFe_2O_4$ was well combined with MoS_2. In addition, the XRD patterns of different ratios of $MoS_2/CuFe_2O_4$ are shown in Fig. S1. The intensity of the (0 0 3) diffraction peak of MoS_2 gradually increased with the weight ratio of MoS_2 in the composite $CuFe_2O_4/MoS_2$.

The surface properties of MoS_2, $CuFe_2O_4$, and $MoS_2/CuFe_2O_4$ were further characterized by using FT-IR (Fig. 1b). The adsorption bands at 484, 904, 950, and 1626 cm^{-1} for MoS_2 sample were derived from the stretching vibration of Mo-—S, S—S bond, Mo═O band, and Mo—O vibration [24,25]. The adsorption band located in 3422 cm^{-1} could be assigned to the stretching of OH groups of adsorbed water [26]. For the pure $CuFe_2O_4$, the signal at 572 cm^{-1} was attributed to the symmetric stretching vibration of the Fe-O band in the tetrahedral FeO_6 groups of spinel-type compounds [27]. Meanwhile, what we could observe was that all the characteristic signals of MoS_2 and $CuFe_2O_4$ were presented in the $MoS_2/CuFe_2O_4$ catalyst, which confirmed the successful synthesis of the composite. As shown in Fig. S2, the N_2 adsorption-desorption isotherms of $CuFe_2O_4$, MoS_2, MC1.5 could be ascribed to type IV curve according to the Brunauer-Deming-Deming-Teller classification. the detailed data about BET surface area, pore diameter, average pore sizes, and pore volume of as-prepared catalysts were listed in the Table S1. Hysteresis loops of type H3 at a relative pressure range of 0.9–1 in pure MoS_2 indicated that the presence of macropores, while Hysteresis loops of type H3 of the pure $CuFe_2O_4$ and modified MC1.5 catalysts was at range of 0.5–1.0, suggesting the presence of mesopores [28]. In addition, the BET surface area of MC1.5 increased after modified, which may mainly due to the addition of $CuFe_2O_4$.

The morphology and structure of MoS_2, $CuFe_2O_4$, and MC1.5 were investigated by field emission-TEM. Fig. 2a shows MoS_2 with a nanosheet structure, which had a dimension of approximately 400 nm. As shown in Fig. 2b, most of the particles of 10 ± 2.3 nm could be seen in the TEM picture of $CuFe_2O_4$, which were slightly aggregated owing to the magnetic effect. However, it can be clearly observed that some nanoparticles were attached to nanosheets (Fig. 2c-d), which was consistent with our assumption that $CuFe_2O_4$ nanoparticles were deposited directly on the surfaces of the MoS_2. Meanwhile, compared with pure $CuFe_2O_4$, there was no significant change about the particle size of $CuFe_2O_4$ on the surface of composite MC1.5 (11 ± 2.6 nm). In addition, the agglomeration of $CuFe_2O_4$ was improved by introducing MoS_2 with lamellar structure. As shown in Fig. S3, by analyzing the zeta potential of as-prepared catalysts, we noticed that $CuFe_2O_4$ lacked stability (|zeta potential| < 30 mv) under pH range from 3 to 8, while MoS_2 was stable due to a high zeta potential (about −50 mv). It is worth noting that the stability of $CuFe_2O_4$ was improved (|zeta potential| > 30 mv) when we doped it on the surface of MoS_2 nanosheets, which might benefit from the reduction of nanoparticles agglomeration. High-resolution transmission electron microscope of MC1.5 (Fig. 2e) showed that the lattice fringes with a spacing of 0.25 nm and 0.61 nm, which could be

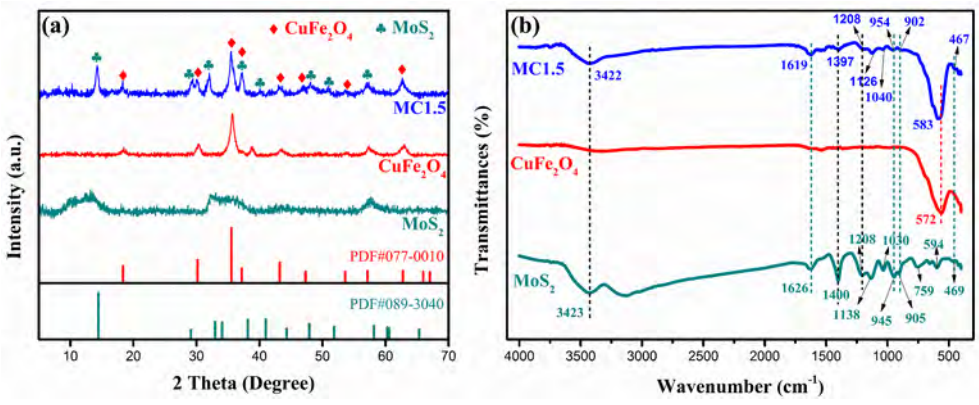

Fig. 1. (a) X-ray diffraction patterns and (b) fourier transform infrared spectra of as-prepared catalysts.

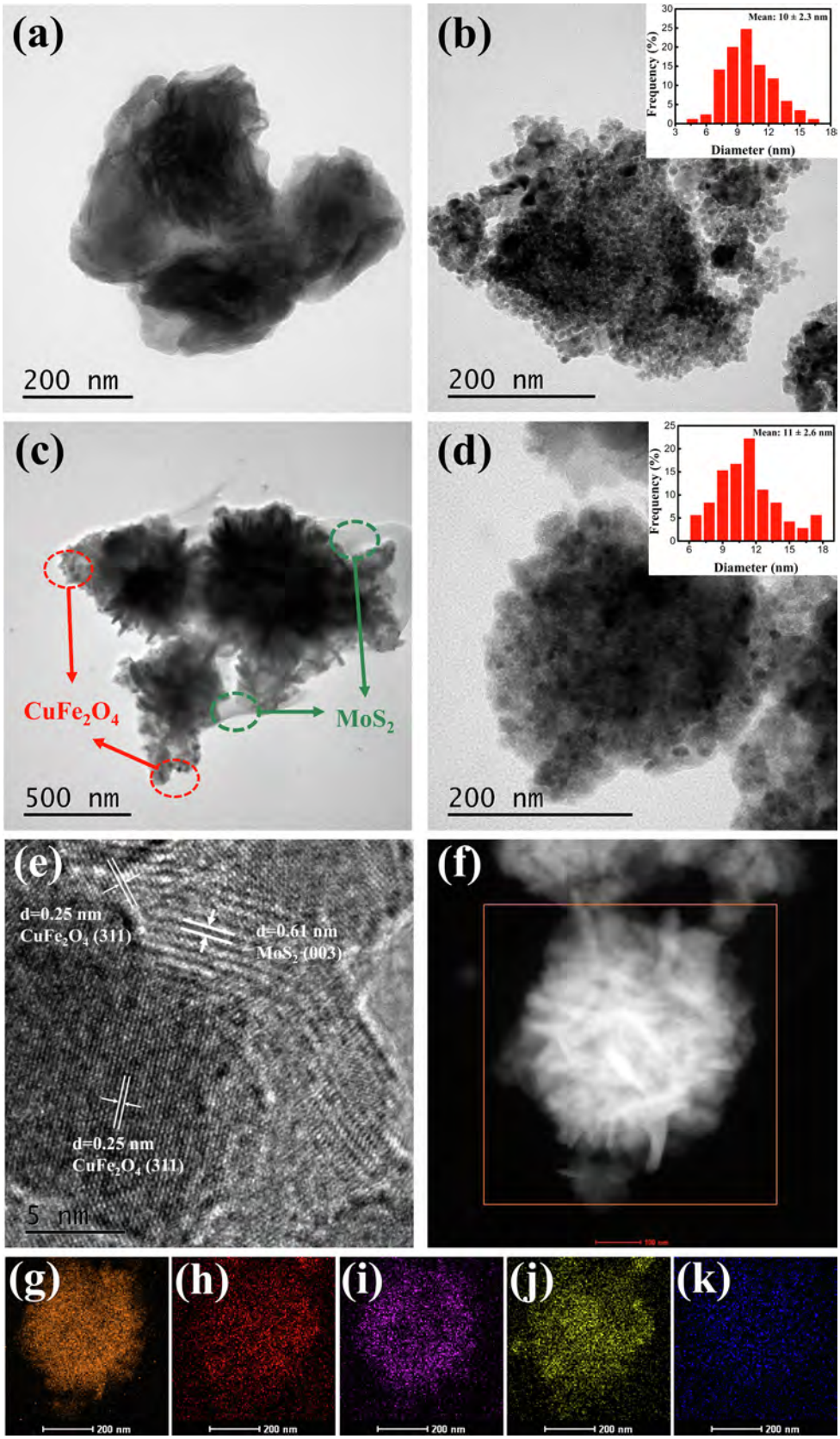

Fig. 2. Transmission electron microscope pictures of (a) MoS_2, (b) $CuFe_2O_4$, and (c-d) MC1.5; (e) high-resolution transmission electron microscope; (f) high angle annular dark-field scanning transmission electron microscope images and corresponding element mapping images of MC1.5 for (g) S, (h) Mo, (i) O, (j) Fe, and (k) Cu. The inset of (b) and (d) is the corresponding particle size distribution of nano-$CuFe_2O_4$.

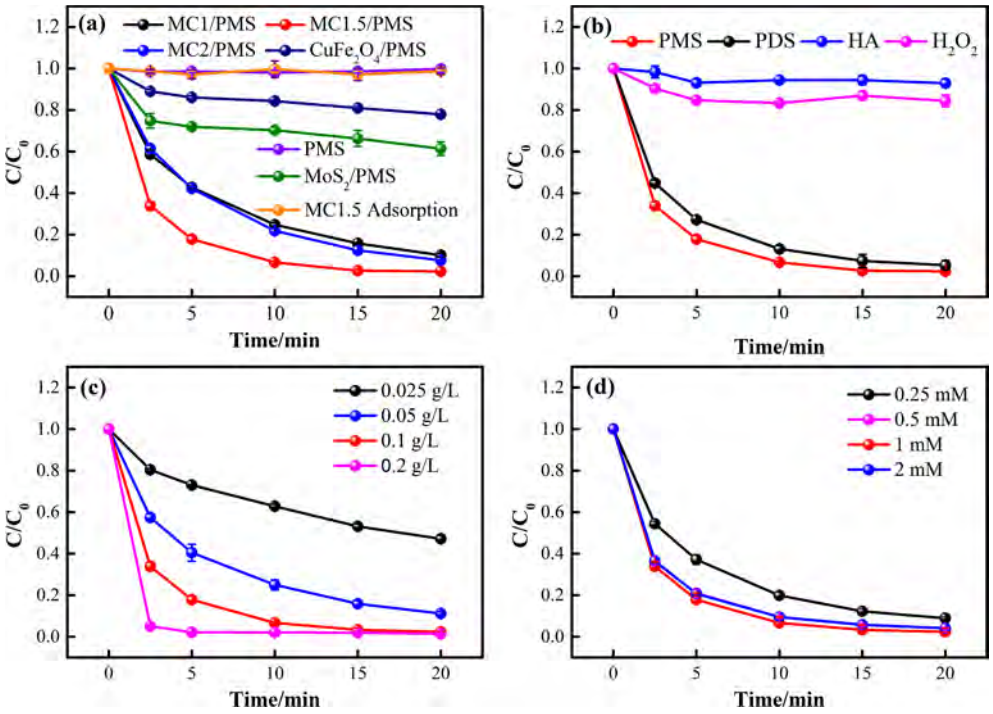

Fig. 3. (a) The degradation efficiency of fluoxetine under various material ratios; the effects of (b) different system, (c) different catalyst dosages, and (d) peroxymonosulfate concentration on the degradation of fluoxetine. Experimental conditions: catalysts = 0.1 g/L, oxidant = 1 mM, initial pH = 6.9, stirring speed = 300 rpm, and T = 25 °C. PMS: peroxymonosulfate; PDS: persulfate; HA: hydroxylamine hydrochloride; H_2O_2: hydrogen peroxide.

attributed to the (3 1 1) plane of $CuFe_2O_4$ and (0 0 3) plane of MoS_2 and were consistent with XRD results. To further verify the above conclusion, energy dispersive spectroscopy mapping was used to investigate the distribution of elements in MC1.5, and showed a uniform distribution of Cu, Fe, O, Mo, and S throughout the catalyst (Fig. 2g–k). In conclusion, $CuFe_2O_4$ was well loaded on the surface of MoS_2.

3.2. Catalytic activity of as-prepared catalysts

3.2.1. Catalytic performance test and condition optimization

As illustrated in Fig. 3a, the result of the addition of peroxymonosulfate and MC1.5 alone showed an imperceptible removal of fluoxetine, thereby suggesting that the contribution of adsorption and the direct oxidation of peroxymonosulfate could be neglected. In addition, $CuFe_2O_4$/peroxymonosulfate and MoS_2/peroxymonosulfate obtained slight degradation of fluoxetine, achieving removal efficiencies of 22.1% and 38.6%, respectively. However, compared with the homogeneous catalyst, $MoS_2/CuFe_2O_4$ as a heterogeneous catalyst showed an excellent effect on the removal of fluoxetine. The composite materials exhibited the best degradation efficiency of 97.7% within 20 min when the molar ratio of MoS_2 to $CuFe_2O_4$ was 1.5:1. The kinetic constants of the first-order kinetics fitting calculations showed that the degradation rate of fluoxetine in the MC1.5/peroxymonosulfate system was 17.6 times and 9.9 times higher than those of $CuFe_2O_4$/peroxymonosulfate and MoS_2/peroxymonosulfate, respectively (Fig. S4a). Simultaneously, different proportions of materials were tested and the results showed that the removal efficiency of fluoxetine reached 92.3% at a ratio of 2:1 and 89.9% at a ratio of 1:1. Therefore, we selected MC1.5 to continue the subsequent experiment.

The removal of fluoxetine was also evaluated in different system, including MC1.5/hydroxylamine, MC1.5/H_2O_2, MC1.5/persulfate and MC1.5/peroxymonosulfate. (Fig. 3b). The removal rate of fluoxetine was negligible in the MC1.5/hydroxylamine and MC1.5/H_2O_2 systems, thereby indicating that MC1.5 could not activate H_2O_2 and persulfate to produce reactive radicals. However, similar to the presence of peroxymonosulfate, MC1.5 also had a good ability to activate persulfate and obtained efficient degradation of fluoxetine. This selectivity with persulfate and peroxymonosulfate by MC1.5 might have been closely related to the addition of MoS_2.

The effect of catalyst dosage on the degradation of fluoxetine by $MoS_2/CuFe_2O_4$/peroxymonosulfate is illustrated in Fig. 3c. There was clear enhancement of the removal of fluoxetine when the concentration of the catalyst MC1.5 was increased from 0.025 g/L to 0.1 g/L. With the dosage of catalyst added to 0.2 g/L, the reaction rate was greatly improved and almost all fluoxetine was removed during about 5 min. This phenomenon occurred because the active site of the catalyst was sufficient to activate peroxymonosulfate and generate radicals to obtain efficient degradation of fluoxetine. Hence, we chose 0.1 g/L of catalyst dosage to carry out the subsequent experiments.

As shown in Fig. 3d, the degradation efficiency improved continuously when the peroxymonosulfate concentration increased from 0.25 to 1 mM, which might have been attributed to the production of free radicals would be improved as the concentration of peroxymonosulfate However, the degradation of fluoxetine underwent a slight decrease when the peroxymonosulfate concentration was increased to 2 mM, which could be explained by the following reasons. On one hand, a limited number of active sites on the surface of the catalyst only activated a certain amount of peroxymonosulfate to generate free radicals. On the other hand, excessive peroxymonosulfate may produce quenching effects because of the reaction between extra HSO_5^- and free radicals ($^{\cdot}OH$ and $SO_4^{\cdot -}$) [29], as described in Eqs. (1–2), as follows:

$$HSO_5^- + SO_4^{\bullet -} \rightarrow SO_5^{\bullet -} + H^+ + SO_4^{2-} \quad (1)$$

$$HSO_5^- + \bullet OH \rightarrow SO_5^{\bullet -} + H_2O \quad (2)$$

Besides, pseudo-first-order kinetics fit the degradation dynamics of fluoxetine well under different process conditions ($R^2 > 0.9$; Fig. S4a–d). By detecting the total organic carbon of samples, we noticed that the mineralization rate of MC1.5/peroxymonosulfate system was about 15% in 20 min (Fig. S5), which may relate to the short reaction time and the stable molecular structure of fluoxetine and its byproducts. This also corresponds to the fact that there are few simple ring-opening products in the analysis of products. In addition, we also tested the reuse performance of MC1.5/peroxymonosulfate (Fig. S6a). MC1.5 showed good stability in the degradation of fluoxetine; after three cycles of degrading fluoxetine, the removal efficiency remained at 83.0%, with a slight decrease from the degradation efficiency of the first cycle

of 97.3%. No new patterns were found in the XRD spectrum of spent catalyst, which was a good evidence that used MC1.5 maintained a high removal capacity (Fig. S6b)

3.2.2. Influence of inorganic ions and natural organic matter

The effects of common inorganic anions (Cl^-, CO_3^{2-}, NO_3^-, SO_4^{2-}, and humic acid) on fluoxetine degradation in the MoS_2/$CuFe_2O_4$/peroxymonosulfate system were also tested (Fig. S7). The addition of Cl^- and CO_3^{2-} exhibited a detrimental effect while NO_3^- and SO_4^{2-} did not have a clear impact on the fluoxetine removal even at a high ion concentration. It was proved that the quenching effect will appear in the system when Cl^- ions are present because Cl^- anions can react with $SO_4^{\cdot -}$ to produce chlorine radicals ($Cl_2^{\cdot -}$), and $Cl_2^{\cdot -}$ also have a lower oxidation potential than that of $SO_4^{\cdot -}$; thus, the oxidation efficiency will be reduced in the presence of Cl^- anions [30,31]. Similarly, a negative impact on fluoxetine degradation was found when the solution contained CO_3^{2-}. This may also occur because CO_3^{2-} anions can react with ·OH and $SO_4^{\cdot -}$ to produce the weaker free radical $CO_3^{\cdot -}$, which may hinder the oxidation of contaminants [32,33]. In addition, humic acid as a common water matrix species was also investigated, and the results suggested that the impact of adding 5, 10, and 20 mg/L of humic acid on fluoxetine degradation can be ignored. Actually, as a representative of natural organic matter, humic acid has a complex role in various degradation systems, and its impact on the degradation systems based on $SO_4^{\cdot -}$ is still unclear. For example, Oh et al. [12] found that the addition of humic acid lead to a significant negative impact on oxidation of bisphenol A in $CuFe_2O_4$–Fe_2O_3/peroxymonosulfate system. However, Li et al. [34] found that the effect of humic acid (8.92 to 44.6 mg/L) on trichloroacetic acid could be ignored, and the addition of humic acid would consume active species in the early reaction (about 30 to 40 min), leading to a lag in the degradation curve. We tend to think it may be related to the concentration of humic acid and reaction time. In our work, the effect of the addition of humic acid was not too significant may be due to the short reaction time (only 20 min) and relatively low concentration of humic acid (5–20 mg/L). The above experiments suggest that MC1.5/peroxymonosulfate has good adaptability to maintain a favorable removal efficiency in the presence of interfering substances.

3.3. Mechanism of peroxymonosulfate activation by MoS_2/$CuFe_2O_4$

The surface composition and oxidation states of the MoS_2/$CuFe_2O_4$ nanocomposites were determined by X-ray photoelectron spectroscopy (XPS). As shown in Fig. 4a, the elements of Cu, Fe, O, Mo, and S

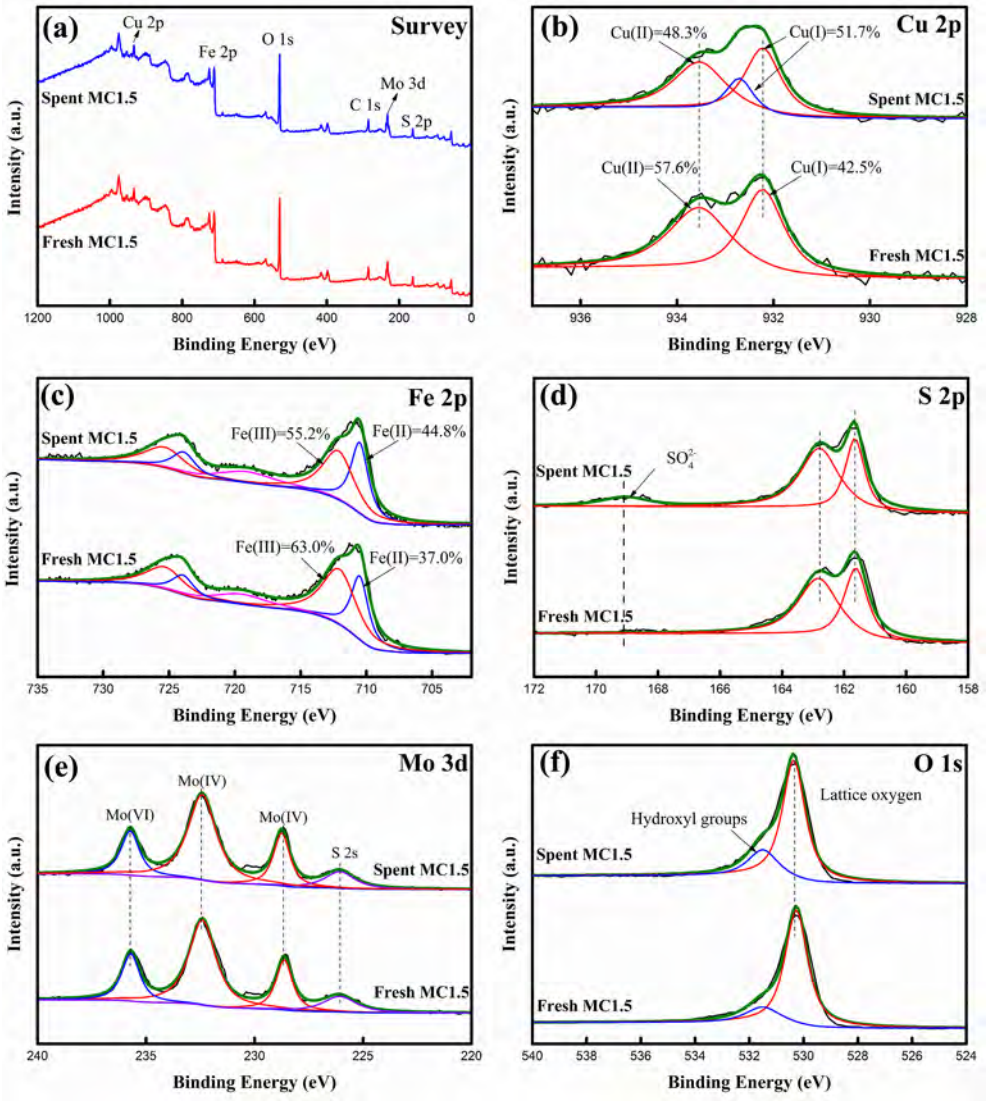

Fig. 4. (a) X-ray photoelectron spectroscopy (XPS) survey, (b) Cu 2p XPS spectra, (c) Fe 2p XPS spectra, (d) S 2p XPS spectra, (e) Mo 3d XPS spectra, and (f) O 1s XPS spectra of MoS_2/$CuFe_2O_4$ before and after the reaction.

coexisted in $MoS_2/CuFe_2O_4$ before and after the reaction. The Cu 2p XPS spectrum displayed two distinct peaks at 932.2 eV and 933.5 eV, which could be ascribed to Cu(I) and Cu(II), respectively (Fig. 4b). In addition, a new peak that occurred at 932.7 eV, which suggested the appearance of a new valence state, could be ascribed to Cu(I) [35]. The proportions of Cu(I) and Cu(II) before the reaction were 36.0% and 50.0%, respectively, while they changed to 57.5% and 42.5% after the reaction, respectively. In addition, a change in the Fe 2p spectrum in the fresh and spent catalysts was found, and two peaks at 710.5 eV and 712.1 eV could be identified as Fe(II) and Fe(III), respectively [36,37] (Fig. 4c). Similar to Cu 2p, the increase in the proportion of Fe(II) was accompanied by a decrease in Fe(III). Regarding S 2p, a peak located at 169.1 eV was observed (Fig. 4d), which could be assigned to SO_4^{2-} ion species.

As shown in Fig. 4e, four clear peaks at 226.1, 228.7, 232.4, and 235.7 eV could be identified as S 2s, Mo(IV), Mo(IV), and Mo(VI), respectively [38]. No clear change in the Mo valence state was observed in the Mo 3d XPS spectrum, thereby suggesting that Mo was stable before and after the reaction. However, this did not mean that Mo was not involved in the formation of free radicals. The large number of defects (unsaturated S) on the surface of the composite material would make Mo more active. Therefore, the stability of the Mo 3d XPS spectrum might have been caused by the formation of Mo(VI), which was immediately reduced to Mo(IV) by peroxymonosulfate [18]. The O 1s XPS spectrum showed two major peaks at 530.2 eV and 531.5 eV before the reaction, which were assigned to the lattice O (O^{2-} from the $CuFe_2O_4$ lattice) and surface hydroxyl group (−OH), respectively [36,39] (Fig. 4f). In addition, the XPS spectra before the reaction clearly suggested the presence of Cu(I), Fe(II), and Mo(VI) within MC1.5, which might have been attributed to the synthesis process that was conducted at a low temperature in an air atmosphere [40].

Furthermore, species quenching experiments were conducted to clarify the mechanism of peroxymonosulfate activation by $MoS_2/CuFe_2O_4$ (Fig. 5a). Generally, methanol is a common scavenger for quenching ·OH ($k = 9.7 \times 10^8\ M^{-1}{\cdot}s^{-1}$) and $SO_4^{\cdot-}$ ($k = 2.5 \times 10^7\ M^{-1}{\cdot}s^{-1}$) [41,42], while *tert*-butanol is used to mainly suppress ·OH because the reaction rate of *tert*-butanol with $SO_4^{\cdot-}$ ($k = 4.0–9.1 \times 10^5\ M^{-1}{\cdot}s^{-1}$) is much lower than that of ·OH ($k = 3.8–7.6 \times 10^8\ M^{-1}{\cdot}s^{-1}$) [42,43]. Clear suppression of the fluoxetine degradation rate, which sharply decreased from 97.7% to 13.5%, was observed after adding 1 mol/L of methanol to the system. Similarly, the addition of 1 mol/L of tert-butanol also led to a clear decline, as the fluoxetine degradation rate dropped to 27%. The results illustrated that $^{\cdot}OH$ and $SO_4^{\cdot-}$ play a major role in the presence of fluoxetine. Meanwhile, they also indicated that $^1O_2$ and $O_2^{\cdot-}$ had a negligible role in this system because the suppression of the addition of methanol was not as clear if these two radicals made a major contribution. In addition, EPR measurements were employed to further clarify the radical oxygen species with DMPO as a spin trapping agent of $^{\cdot}OH$ and $SO_4^{\cdot-}$ [44]. As shown in Fig. 5b, the EPR spectra of the 1:2:2:1 peak signal was obtained, which is the typical signal for DMPO-·OH. Meanwhile, some weak signals surrounding these four peaks could be assigned to DMPO-$SO_4^{\cdot-}$. The above results were consistent with the species quenching experiments, which implied that $MoS_2/CuFe_2O_4$ can effectively activate peroxymonosulfate to generate ·OH and $SO_4^{\cdot-}$. In addition, low-temperature EPR spectra of MC1.5 showed a strong signal at g = 2.0, indicating that a number of S vacancies were on the surface of composite materials (Fig. 5c), which made the catalyst more active and further promoted the reaction rate [16].

In addition, the peroxymonosulfate molecules were determined by in situ Roman spectra (Fig. 5d), and three peaks at 884, 983, and 1062 cm^{-1} were observed, which represented HSO_5^-, SO_4^{2-}, and HSO_5^-, respectively [45,46]. Meanwhile, I_{1062}/I_{983} could also be used to estimate the decomposition of peroxymonosulfate [47], and the ratio was 0.95 in the peroxymonosulfate system. However, the figure decreased to 0.93 and 0.71 when the experiment was conducted in the $CuFe_2O_4$/peroxymonosulfate system and MoS_2/peroxymonosulfate system, respectively, which indicated that the introduction of MoS_2 accelerated the consumption of peroxymonosulfate molecules. In addition, a lower value of I_{1062}/I_{983} (0.62) occurred in the presence of MC1.5, thereby illustrating that HSO_5^- was converted to SO_4^{2-} at a faster rate.

According to the above results, mechanisms of $MoS_2/CuFe_2O_4$ activation of peroxymonosulfate for rapid degradation of fluoxetine were proposed (Fig. 6). First, Cu(I) and Fe(II) on the catalyst surface could directly contribute to the formation of free radicals (Eqs. (3)–(5)) [27],

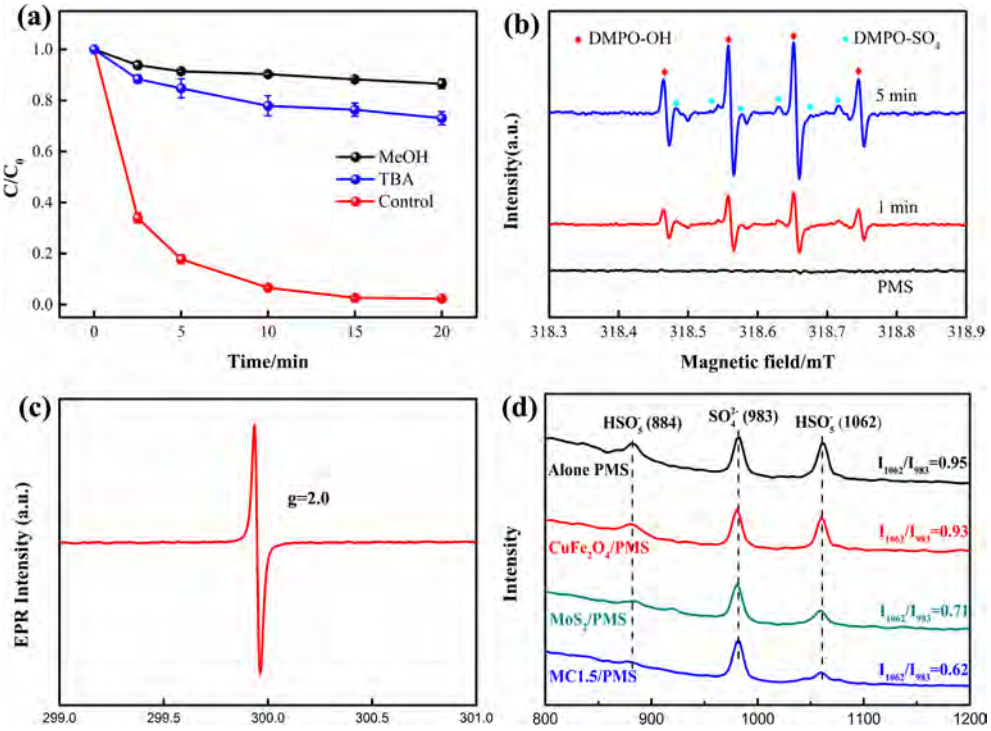

Fig. 5. (a) Effects of the scavengers (MeOH: methanol; TBA: *tert*-butanol); (b) DMPO-·OH and DMPO-$SO_4^{\cdot-}$ adducts signal intensity detected by electron paramagnetic resonance (EPR) under room temperature ($[fluoxetine]_0$ = 20 mg/L, $[catalyst]_0$ = 0.1 g/L, $[peroxymonosulfate]_0$ = 1 mM, initial pH = 6.9, stirring speed = 300 rpm, and T = 25 °C.); (c) low-temperature EPR spectra of MC1.5; and (d) Raman spectra recorded from MC1.5/PMS, $CuFe_2O_4$/PMS, MoS_2/PMS, and PMS solutions ($[catalyst]_0$ = 2.0 g/L, $[peroxymonosulfate]_0$ = 20 mM, stirring speed = 300 rpm, and T = 25 °C; PMS: peroxymonosulfate).

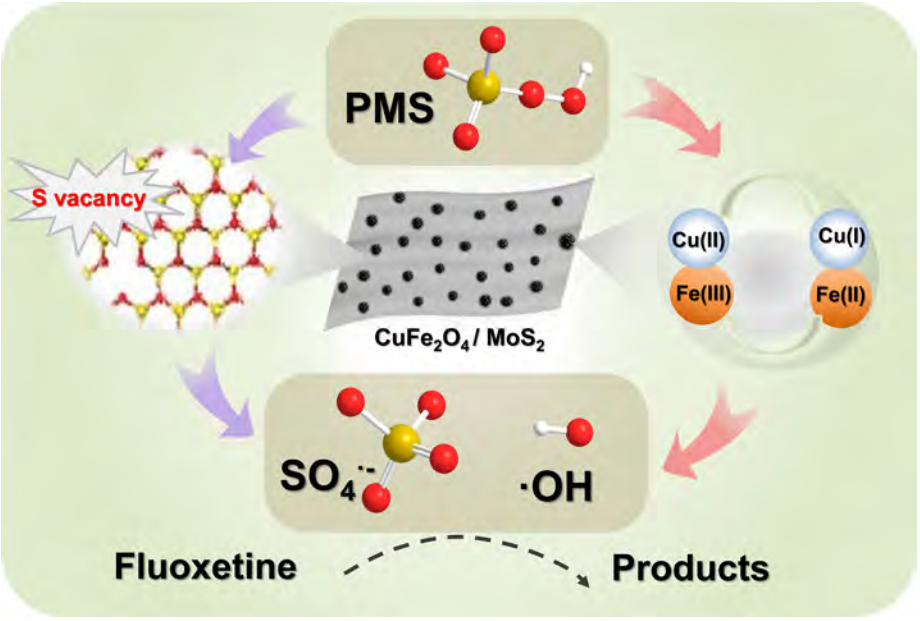

Fig. 6. Proposed generation mechanism of radicals in the MoS_2/$CuFe_2O_4$/peroxymonosulfate system.

which was clearly proved by the change in the proportion of elements before and after the experiment from the XPS spectrum. Meanwhile, compared with the pure MoS_2, highly dispersed $CuFe_2O_4$ nanoparticles on the surface of composite material could increase its specific surface area and further facilitate the contact probability between the catalyst and the oxidant, thus promoting the efficient activation of peroxymonosulfate also contributed to the improvement of the reaction rate. Second, the composite material with a large number of defects was bound to have a certain reduction property, which could adsorb the peroxymonosulfate molecules and further accelerate the electron transfer efficiency between the oxidant and the material surface. Deng et al. [48] revealed that surface active sites could enhance the adsorption of hydroxyl molecules on the surface of iron-doped ordered mesoporous Co_3O_4, which was conducive to the transfer of electrons from Co^{2+}/Co^{3+} and Fe^{2+}/Fe^{3+} to peroxymonosulfate and decomposition of peroxymonosulfate. Recently, Chen et al. [45] made use of theoretical calculations to predict that MoS_2 has a significant affinity for key intermediates during the activation of peroxymonosulfate, which could be well confirmed by the appearance of sulfate species on the S 2p XPS spectrum after the reaction. Hence, the metal elements near S vacancies would become active because of the presence of defects, and electrons could transfer on the catalyst surface through the pathway of Metal-S Vacancy-Peroxymonosulfate molecule, participating in the decomposition of peroxymonosulfate to generate the free radical.

$$\equiv Cu(I)/Fe(II) + HSO_5^- \rightarrow \equiv Cu(II)/Fe(III) + SO_4^{2-} + \bullet OH \quad (3)$$

$$\equiv Cu(I)/Fe(II) + HSO_5^- \rightarrow \equiv Cu(II)/Fe(III) + SO_4^{2-} + OH^- \quad (4)$$

$$\equiv Cu(II)/Fe(III) + HSO_5^- \rightarrow \equiv Cu(I)/Fe(II) + SO_5^{\bullet-} + H^+ \quad (5)$$

3.4. Proposed transformation pathway of fluoxetine

The byproducts of fluoxetine degraded by MoS_2/$CuFe_2O_4$/peroxymonosulfate were identified using Q Exactive MS, and the intermediates were analyzed in both ESI+ and ESI- mode. Nine products (compounds P1–P9) caused by ·OH and $SO_4^{\cdot-}$ were detected, which mainly involved a chain breaking reaction, hydroxylation reaction, and ring opening reaction. The potential intermediates and proposed transformation pathways are shown in Fig. 7 and Table S3.

The C-O bond of fluoxetine molecules was easily broken owing to the attack of ·OH and $SO_4^{\cdot-}$, which led to the occurrence of a chain cleavage reaction to generate compounds P1 ($[M-H]^-$ at m/z 161; $C_7H_5F_3O$), P2 ($[M+H]^+$ at m/z 166; $C_{10}H_{15}NO$), and P3 ($[M+H]^+$ at m/z 164; $C_{10}H_{13}NO$). Mendez-Arriaga et al. also detected the product P2 in a TiO_2-photoassisted degradation fluoxetine system [49]. Recently, Selina et al. also identified the product P1 using ESI- mode during photodegradation [50]. In our degradation system, a variety of hydroxylation products related to compound P1 were detected, including P7 ($[M-H]^-$ at m/z 177; $C_7H_5F_3O_2$) and P8 ($[M-H]^-$ at m/z 209; $C_7H_5F_3O_4$). In addition, we also found a ring opening product (P9: $[M-H]^-$ at m/z 185; $C_5H_5F_3O_4$), which might have been driven by the ring cleavage reaction of compound P7.

In addition, plenty of ·OH in the MoS_2/$CuFe_2O_4$/peroxymonosulfate system also tended to be added to the fluoxetine molecules, which could have resulted from the generation of hydroxylated molecule P4 ($[M-H]^-$ at m/z 324; $C_{17}H_{18}F_3NO_2$). This is a typical intermediate in the fluoxetine degradation system [51], and the ·OH tends to be added first to the benzene ring further from the O atom. Meanwhile, this hydroxylated fluoxetine (compound P4) was more active than the original fluoxetine molecule, which could not only be further hydroxylated to form a more complex molecule (P5: $[M+H]^+$ at m/z 388; $C_{17}H_{18}F_3NO_6$), but also be oxidized to compounds P1, P2, and P3 by a chain cleavage reaction. In addition, the byproduct P6 ($[M+H]^+$ at m/z 260; $C_{12}H_{12}F_3NO_2$) generated from P4 could be explained by the loss of the methyl group and opening of the benzene ring, which was also detected in the ozonation of fluoxetine in a previous study conducted by Zhao et al.[21]. The MS/MS spectra regarding all the above intermediate products and the analysis of fragment ions generated by secondary MS are shown in Figs. S8–16.

4. Conclusion

Based on all the results about the degradation of fluoxetine through the MoS_2/$CuFe_2O_4$/peroxymonosulfate system, the conclusions were as follows:

(1) The use of a two-step hydrothermal method to prepare MoS_2/$CuFe_2O_4$ catalysts with different mass ratios and the characterization of low-temperature EPR suggested that abundant S vacancies were present on the surface of the composite catalyst.

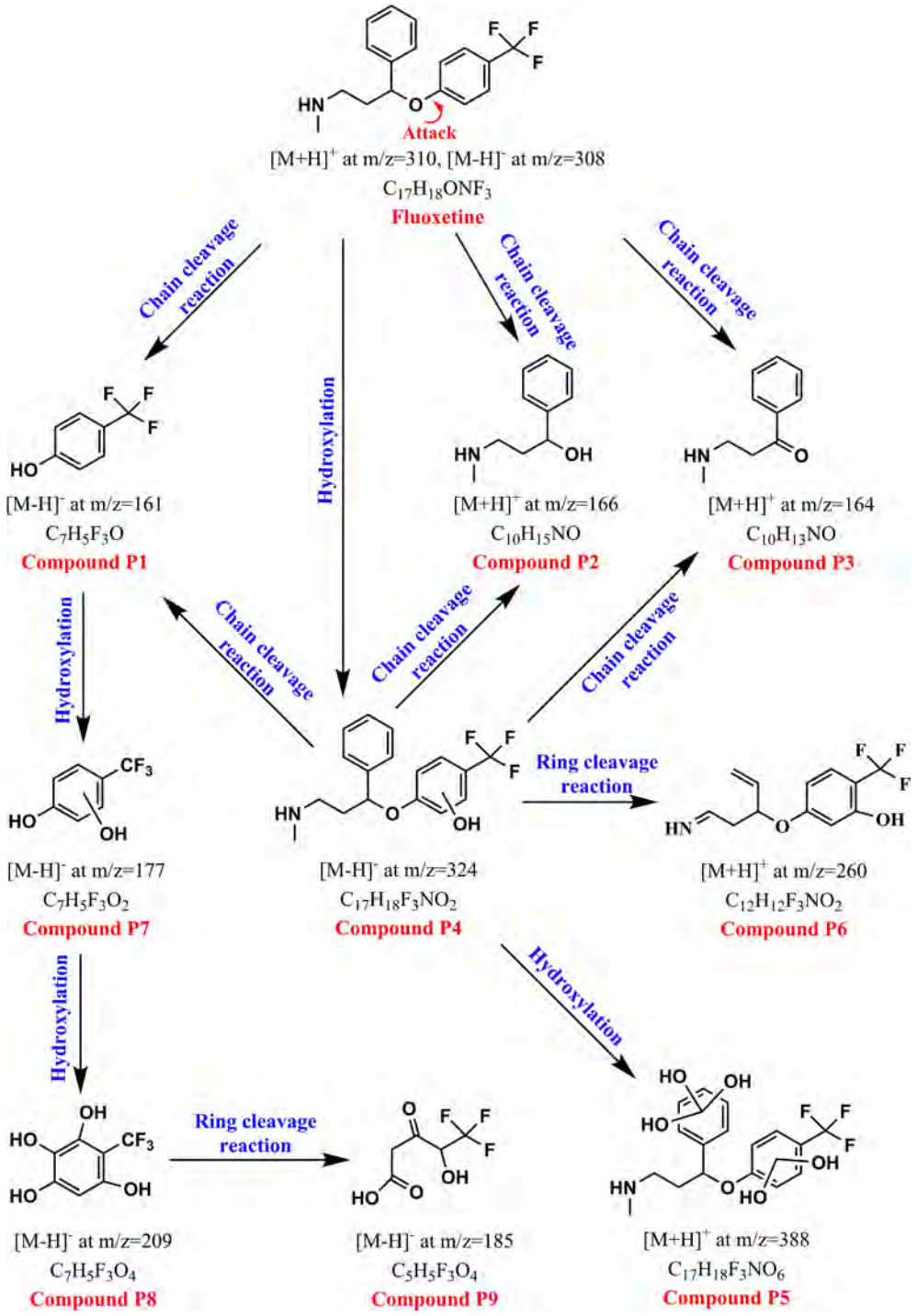

Fig. 7. Structures of intermediates and proposed reaction sequence for the degradation of fluoxetine under the $MoS_2/CuFe_2O_4$/peroxymonosulfate system.

(2) The compound catalyst MC1.5/peroxymonosulfate system showed the highest removal rate for fluoxetine, which was 17.6 times and 9.9 times higher than those of the $CuFe_2O_4$/peroxymonosulfate and MoS_2/peroxymonosulfate systems, respectively.
(3) The EPR and radical scavenging experiments indicated that $^{\cdot}OH$ and $SO_4^{\cdot -}$ played major roles in the MC1.5/peroxymonosulfate system.
(4) The results based on in situ Roman spectra and the XPS spectra of MC1.5 before and after the reaction illustrated the mechanism of electron transfer between peroxymonosulfate and $MoS_2/CuFe_2O_4$.
(5) HPLC-MS/MS analysis showed that nine degradation intermediates were driven by breaking of C-O bonds, hydroxylation, and ring opening of fluoxetine.

Our study provides a scientific reference for the further design of new Mo-based multiphase catalysts, and has significance for the degradation analysis of fluoxetine.

Declaration of Competing Interest

The authors declare that they have no known competing financial interests or personal relationships that could have appeared to influence the work reported in this paper.

Acknowledgements

This study was supported by grants from the National Natural Science Foundation of China (51878640), the Youth Innovation Promotion Association of Chinese Academy of Sciences (2018344) and the FJIRSM&IUE Joint Research Fund (RHZX-2018-006).

Appendix A. Supplementary data

Supplementary data to this article can be found online at https://doi.org/10.1016/j.cej.2020.125501.

References

[1] R.P. Schwarzenbach, B.I. Escher, K. Fenner, T.B. Hofstetter, C.A. Johnson, U. von Gunten, B. Wehrli, The challenge of micropollutants in aquatic systems, Science 313 (2006) 1072–1077, https://doi.org/10.1126/science.1127291.

[2] A.B.A. Boxall, M.A. Rudd, B.W. Brooks, D.J. Caldwell, K. Choi, S. Hickmann, E. Innes, K. Ostapyk, J.P. Staveley, T. Verslycke, G.T. Ankley, K.F. Beazley, S.E. Belanger, J.P. Berninger, P. Carriquiriborde, A. Coors, P.C. DeLeo, S.D. Dyer, J.F. Ericson, F. Gagne, J.P. Giesy, T. Gouin, L. Hallstrom, M.V. Karlsson, D.G.J. Larsson, J.M. Lazorchak, F. Mastrocco, A. McLaughlin, M.E. McMaster, R.D. Meyerhoff, R. Moore, J.L. Parrott, J.R. Snape, R. Murray-Smith, M.R. Servos, P.K. Sibley, J.O. Straub, N.D. Szabo, E. Topp, G.R. Tetreault, V.L. Trudeau, G. Van Der Kraak, Pharmaceuticals and personal care products in the environment: What are the big questions? Environ. Health Persp 120 (2012) 1221–1229, https://doi.org/10.1289/ehp.1104477.

[3] M. Gust, T. Buronfosse, L. Giamberini, M. Ramil, R. Mons, J. Garric, Effects of fluoxetine on the reproduction of two prosobranch mollusks: Potamopyrgus antipodarum and Valvata piscinalis, Environ. Pollut. 157 (2009) 423–429, https://doi.org/10.1016/j.envpol.2008.09.040.

[4] J.-L. Liu, M.-H. Wong, Pharmaceuticals and personal care products (PPCPs): a review on environmental contamination in China, Environ. Int. 59 (2013) 208–224, https://doi.org/10.1016/j.envint.2013.06.012.

[5] R. Andreozzi, V. Caprio, A. Insola, R. Marotta, Advanced oxidation processes (AOP) for water purification and recovery, Catal. Today 53 (1999) 51–59, https://doi.org/10.1016/S0920-5861(99)00102-9.

[6] H. Li, C. Shan, B. Pan, Fe(III)-doped g-C_3N_4 mediated peroxymonosulfate activation for selective degradation of phenolic compounds via high-valent iron-oxo species, Environ. Sci. Technol. 52 (2018) 2197–2205, https://doi.org/10.1021/acs.est.7b05563.

[7] X. Duan, C. Su, J. Miao, Y. Zhong, Z. Shao, S. Wang, H. Sun, Insights into perovskite-catalyzed peroxymonosulfate activation: Maneuverable cobalt sites for promoted evolution of sulfate radicals, Appl. Catal. B-Environ. 220 (2018) 626–634, https://doi.org/10.1016/j.apcatb.2017.08.088.

[8] Y.-H. Guan, J. Ma, X.-C. Li, J.-Y. Fang, L.-W. Chen, Influence of pH on the formation of sulfate and hydroxyl radicals in the UV/peroxymonosulfate system, Environ. Sci. Technol. 45 (2011) 9308–9314, https://doi.org/10.1021/es2017363.

[9] Y. Ji, C. Dong, D. Kong, J. Lu, Q. Zhou, Heat-activated persulfate oxidation of atrazine: Implications for remediation of groundwater contaminated by herbicides, Chem. Eng. J. 263 (2015) 45–54, https://doi.org/10.1016/j.cej.2014.10.097.

[10] C. Cai, H. Zhang, X. Zhong, L. Hou, Ultrasound enhanced heterogeneous activation of peroxymonosulfate by a bimetallic Fe–Co/SBA-15 catalyst for the degradation of Orange II in water, J. Hazard. Mater. 283 (2015) 70–79, https://doi.org/10.1016/j.jhazmat.2014.08.053.

[11] X. Cheng, H. Liang, A. Ding, X. Zhu, X. Tang, Z. Gan, J. Xing, D. Wu, G. Li, Application of Fe(II)/peroxymonosulfate for improving ultrafiltration membrane performance in surface water treatment: Comparison with coagulation and ozonation, Water Res. 124 (2017) 298–307, https://doi.org/10.1016/j.watres.2017.07.062.

[12] W.-D. Oh, Z. Dong, Z.-T. Hu, T.-T. Lim, A novel quasi-cubic $CuFe_2O_4$-Fe_2O_3 catalyst prepared at low temperature for enhanced oxidation of bisphenol A via peroxymonosulfate activation, J. Mater. Chem. A 3 (2015) 22208–22217, https://doi.org/10.1039/c5ta06563a.

[13] Z.Z. Liu, Y.Z. Guo, R. Shang, Z. Fang, F. Wu, Z.P. Wang, A triple system of Fe(III)/sulfite/persulfate: decolorization and mineralization of reactive Brilliant Red X-3B in aqueous solution at near-neutral pH values, J. Taiwan Inst. Chem. Eng. 68 (2016) 162–168, https://doi.org/10.1016/j.jtice.2016.08.027.

[14] J. Li, Y. Ren, F. Ji, B. Lai, Heterogeneous catalytic oxidation for the degradation of p-nitrophenol in aqueous solution by persulfate activated with $CuFe_2O_4$ magnetic nano-particles, Chem. Eng. J. 324 (2017) 63–73, https://doi.org/10.1016/j.cej.2017.04.104.

[15] J. Yang, D. Wang, H. Han, C. Li, Roles of cocatalysts in photocatalysis and photoelectrocatalysis, Accounts. Chem. Res. 46 (2013) 1900–1909, https://doi.org/10.1021/ar300227e.

[16] M. Xing, W. Xu, C. Dong, Y. Bai, J. Zeng, Y. Zhou, J. Zhang, Y. Yin, Metal sulfides as excellent co-catalysts for H_2O_2 decomposition in advanced oxidation processes, Chem 4 (2018) 1359–1372, https://doi.org/10.1016/j.chempr.2018.03.002.

[17] J. Liu, C. Dong, Y. Deng, J. Ji, S. Bao, C. Chen, B. Shen, J. Zhang, M. Xing, Molybdenum sulfide Co-catalytic Fenton reaction for rapid and efficient inactivation of Escherichia coli, Water Res. 145 (2018) 312–320, https://doi.org/10.1016/j.watres.2018.08.039.

[18] B. Sheng, F. Yang, Y. Wang, Z. Wang, Q. Li, Y. Guo, X. Lou, J. Liu, Pivotal roles of MoS_2 in boosting catalytic degradation of aqueous organic pollutants by Fe(II)/PMS, Chem. Eng. J. 375 (2019) 121989, , https://doi.org/10.1016/j.cej.2019.121989.

[19] Z. Wang, B. Mi, Environmental applications of 2D molybdenum disulfide (MoS_2) nanosheets, Environ. Sci. Technol. 51 (2017) 8229–8244, https://doi.org/10.1021/acs.est.7b01466.

[20] L. Zeng, S. Li, X. Li, J. Li, S. Fan, X. Chen, Z. Yin, M. Tadé, S. Liu, Visible-light-driven sonophotocatalysis and peroxymonosulfate activation over 3D urchin-like MoS_2/C nanoparticles for accelerating levofloxacin elimination: Optimization and kinetic study, Chem. Eng. J. 378 (2019) 122039, , https://doi.org/10.1016/j.cej.2019.122039.

[21] Y. Zhao, G. Yu, S. Chen, S. Zhang, B. Wang, J. Huang, S. Deng, Y. Wang, Ozonation of antidepressant fluoxetine and its metabolite product norfluoxetine: kinetics, intermediates and toxicity, Chem. Eng. J. 316 (2017) 951–963, https://doi.org/10.1016/j.cej.2017.02.032.

[22] R. Bai, Y. Xiao, W.F. Yan, S.Q. Wang, R. Ding, F. Yang, J.P. Li, X.Q. Lu, F. Zhao, Rapid and efficient removal of naproxen from water by $CuFe_2O_4$ with peroxymonosulfate, Environ. Sci. Pollut. R. (2020), https://doi.org/10.1007/s11356-020-08613-7.

[23] Y. Zeng, N. Guo, Y. Song, Y. Zhao, H. Li, X. Xu, J. Qiu, H. Yu, Fabrication of Z-scheme magnetic MoS_2/$CoFe_2O_4$ nanocomposites with highly efficient photocatalytic activity, J. Colloid Interf. Sci 514 (2018) 664–674, https://doi.org/10.1016/j.jcis.2017.12.079.

[24] H. Akram, C. Mateos-Pedrero, E. Gallegos-Suárez, A. Guerrero-Ruíz, T. Chafik, I. Rodríguez-Ramos, Effect of electrolytes nature and concentration on the morphology and structure of MoS_2 nanomaterials prepared using one-pot solvothermal method, Appl. Surf. Sci. 307 (2014) 319–326, https://doi.org/10.1016/j.apsusc.2014.04.034.

[25] Y. Song, K. Cao, W. Li, C. Ma, X. Qiao, H. Li, C. Hong, Optimal film thickness of rGO/MoS_2@polyaniline nanosheets of 3D arrays for carcinoembryonic antigen high sensitivity detection, Microchem. J. 155 (2020) 104694, , https://doi.org/10.1016/j.microc.2020.104694.

[26] S. Xing, C. Hu, J. Qu, H. He, M. Yang, Characterization and reactivity of MnOx supported on mesoporous Zirconia for herbicide 2,4-D mineralization with ozone, Environ. Sci. Technol. 42 (2008) 3363–3368, https://doi.org/10.1021/es0718671.

[27] Y. Ding, L. Zhu, N. Wang, H. Tang, Sulfate radicals induced degradation of tetrabromobisphenol A with nanoscaled magnetic $CuFe_2O_4$ as a heterogeneous catalyst of peroxymonosulfate, Appl. Catal. B-Environ. 129 (2013) 153–162, https://doi.org/10.1016/j.apcatb.2012.09.015.

[28] Y. Min, G. He, Q. Xu, Y. Chen, Dual-functional MoS_2 sheet-modified CdS branch-like heterostructures with enhanced photostability and photocatalytic activity, J. Mater. Chem. A 2 (2014) 2578–2584, https://doi.org/10.1039/C3TA14240J.

[29] Y. Xu, J. Ai, H. Zhang, The mechanism of degradation of bisphenol A using the magnetically separable $CuFe_2O_4$/peroxymonosulfate heterogeneous oxidation process, J. Hazard. Mater. 309 (2016) 87–96, https://doi.org/10.1016/j.jhazmat.2016.01.023.

[30] W.-D. Oh, S.-K. Lua, Z. Dong, T.-T. Lim, A novel three-dimensional spherical $CuBi_2O_4$ consisting of nanocolumn arrays with persulfate and peroxymonosulfate activation functionalities for 1H-benzotriazole removal, Nanoscale 7 (2015) 8149–8158, https://doi.org/10.1039/C5NR01428J.

[31] T. Zhang, H. Zhu, J.-P. Croué, Production of sulfate radical from peroxymonosulfate induced by a magnetically separable $CuFe_2O_4$ spinel in water: efficiency, stability, and mechanism, Environ. Sci. Technol. 47 (2013) 2784–2791, https://doi.org/10.1021/es304721g.

[32] T. Zhou, X. Zou, J. Mao, X. Wu, Decomposition of sulfadiazine in a sonochemical Fe^0-catalyzed persulfate system: parameters optimizing and interferences of wastewater matrix, Appl. Catal. B-Environ. 185 (2016) 31–41, https://doi.org/10.1016/j.apcatb.2015.12.004.

[33] C. Liang, Z.-S. Wang, N. Mohanty, Influences of carbonate and chloride ions on persulfate oxidation of trichloroethylene at 20 °C, Sci. Total. Environ. 370 (2006) 271–277, https://doi.org/10.1016/j.scitotenv.2006.08.028.

[34] B. Li, L. Li, K. Lin, W. Zhang, S. Lu, Q. Luo, Removal of 1,1,1-trichloroethane from aqueous solution by a sono-activated persulfate process, Ultrason. Sonochem. 20 (2013) 855–863, https://doi.org/10.1016/j.ultsonch.2012.11.014.

[35] J. Li, J. Zeng, L. Jia, W. Fang, Investigations on the effect of Cu^{2+}/Cu^{1+} redox couples and oxygen vacancies on photocatalytic activity of treated $LaNi_{1-x}Cu_xO_3$ (x = 0.1, 0.4, 0.5), Int. J. Hydrogen Energ 35 (2010) 12733–12740, https://doi.org/10.1016/j.ijhydene.2010.08.140.

[36] Y. Yao, F. Lu, Y. Zhu, F. Wei, X. Liu, C. Lian, S. Wang, Magnetic core–shell $CuFe_2O_4$@C_3N_4 hybrids for visible light photocatalysis of Orange II, J. Hazard. Mater. 297 (2015) 224–233, https://doi.org/10.1016/j.jhazmat.2015.04.046.

[37] R. Rajendiran, D. Chinnadurai, A.R. Selvaraj, R.K. Gunasekaran, H.-J. Kim, S. Karupannan, K. Prabakar, Nickel self-doped iron oxide/manganese carbonate hierarchical 2D/3D structures for electrochemical energy storage, Electrochim. Acta 297 (2019) 77–86, https://doi.org/10.1016/j.electacta.2018.11.177.

[38] Y. Jia, H. Ma, C. Liu, Au nanoparticles enhanced Z-scheme Au-$CoFe_2O_4$/MoS_2 visible light photocatalyst with magnetic retrievability, Appl. Surf. Sci. 463 (2019) 854–862, https://doi.org/10.1016/j.apsusc.2018.09.008.

[39] F. Qi, W. Chu, B. Xu, Ozonation of phenacetin in associated with a magnetic catalyst $CuFe_2O_4$: the reaction and transformation, Chem. Eng. J. 262 (2015) 552–562, https://doi.org/10.1016/j.cej.2014.09.068.

[40] R. Li, M. Cai, Z. Xie, Q. Zhang, Y. Zeng, H. Liu, G. Liu, W. Lv, Construction of heterostructured $CuFe_2O_4$/g-C_3N_4 nanocomposite as an efficient visible light photocatalyst with peroxydisulfate for the organic oxidation, Appl. Catal. B-Environ.

244 (2019) 974–982, https://doi.org/10.1016/j.apcatb.2018.12.043.
[41] G.V. Buxton, C.L. Greenstock, W.P. Helman, A.B. Ross, Critical review of rate constants for reactions of hydrated electrons, hydrogen atoms and hydroxyl radicals (·OH/·O−) in aqueous solution, J. Phys. Chem. Ref. Data 17 (1988) 513–886, https://doi.org/10.1063/1.555805.
[42] P. Neta, R.E. Huie, A.B. Ross, Rate constants for reactions of inorganic radicals in aqueous solution, J. Phys. Chem. Ref. Data 17 (1988) 1027–1284, https://doi.org/10.1063/1.555808.
[43] G.P. Anipsitakis, D.D. Dionysiou, Radical generation by the interaction of transition metals with common oxidants, Environ. Sci. Technol. 38 (2004) 3705–3712, https://doi.org/10.1021/es035121o.
[44] J. Zou, J. Ma, L.W. Chen, X.C. Li, Y.H. Guan, P.C. Xie, C. Pan, Rapid acceleration of ferrous iron/peroxymonosulfate oxidation of organic pollutants by promoting Fe (III)/Fe(II) cycle with hydroxylamine, Environ. Sci. Technol. 47 (2013) 11685–11691, https://doi.org/10.1021/es4019145.
[45] Y. Chen, G. Zhang, H. Liu, J. Qu, Confining free radicals in close vicinity to contaminants enables ultrafast Fenton-like processes in the interspacing of MoS_2 membranes, Angew. Chem.-Int. Edit. 58 (2019) 8134–8138, https://doi.org/10.1002/anie.201903531.
[46] J.-C.E. Yang, B. Yuan, H.-J. Cui, S. Wang, M.-L. Fu, Modulating oxone-MnOx/silica catalytic systems towards ibuprofen degradation: Insights into system effects, reaction kinetics and mechanisms, Appl. Catal. B-Environ. 205 (2017) 327–339, https://doi.org/10.1016/j.apcatb.2016.12.046.
[47] L. Yu, G. Zhang, C. Liu, H. Lan, H. Liu, J. Qu, Interface stabilization of under-coordinated iron centers on manganese oxides for nature-inspired peroxide activation, ACS Catalysis 8 (2018) 1090–1096, https://doi.org/10.1021/acscatal.7b03338.
[48] J. Deng, M. Xu, S. Feng, C. Qiu, X. Li, J. Li, Iron-doped ordered mesoporous Co_3O_4 activation of peroxymonosulfate for ciprofloxacin degradation: Performance, mechanism and degradation pathway, Sci. Total. Environ. 658 (2019) 343–356, https://doi.org/10.1016/j.scitotenv.2018.12.187.
[49] F. Méndez-Arriaga, T. Otsu, T. Oyama, J. Gimenez, S. Esplugas, H. Hidaka, N. Serpone, Photooxidation of the antidepressant drug Fluoxetine (Prozac®) in aqueous media by hybrid catalytic/ozonation processes, Water Res. 45 (2011) 2782–2794, https://doi.org/10.1016/j.watres.2011.02.030.
[50] S. Tisler, F. Zindler, F. Freeling, K. Nödler, L. Toelgyesi, T. Braunbeck, C. Zwiener, Transformation products of fluoxetine formed by photodegradation in water and biodegradation in Zebrafish Embryos (Danio rerio), Environ. Sci. Technol. 53 (2019) 7400–7409, https://doi.org/10.1021/acs.est.9b00789.
[51] V.H.O. Silva, A.P. dos Santos Batista, A.C. Silva Costa Teixeira, S.I. Borrely, Degradation and acute toxicity removal of the antidepressant Fluoxetine (Prozac®) in aqueous systems by electron beam irradiation, Environ. Sci. Pollut. R 23 (2016) 11927–11936, https://doi.org/10.1007/s11356-016-6410-1.